Collective and noncollective states in ^{116}Sb

S. Y. Wang(王守宇),[1,*] D. P. Sun(孙大鹏),[1] B. Qi(亓斌),[1] Z. Q. Chen(陈志强),[1] X. B. Hu(胡孝斌),[1] G. Wang(王庚),[1] C. Liu(刘晨),[1] C. J. Xu(徐长江),[1] L. Liu(刘雷),[1] P. Zhang(张盼),[1] Z. Q. Li(李志泉),[1] M. Z. Guo(郭明哲),[1] Y. Y. Cai(蔡杨杨),[1] Y. Q. Li(李昱琪),[1] S. Y. Liu(刘尚源),[1] S. M. Wyngaardt,[2] L. H. Zhu(竺礼华),[3] X. G. Wu(吴晓光),[4] C. Y. He(贺创业),[4] Y. Zheng(郑云),[4] and G. S. Li(李广生)[4]

[1]*Shandong Provincial Key Laboratory of Optical Astronomy and Solar-Terrestrial Environment, School of Space Science and Physics, Shandong University, Weihai 264209, People's Republic of China*

[2]*Department of Physics, University of Stellenbosch, Matieland 7602, South Africa*

[3]*School of Physics and Nuclear Energy Engineering, Beihang University, Beijing 100191, People's Republic of China*

[4]*China Institute of Atomic Energy, Beijing 102413, People's Republic of China*

(Received 31 August 2012; revised manuscript received 17 October 2012; published 4 December 2012)

Excited states of ^{116}Sb were investigated using in-beam γ-ray spectroscopy techniques with the ^{114}Cd(^{7}Li, $5n$) reaction. About 25 new states and 35 new transitions were added into the level scheme of ^{116}Sb. The previously known two rotational bands based on the $\pi g_{9/2}{}^{-1} \otimes \nu h_{11/2}$ and $\pi g_{9/2}{}^{-1} \otimes \nu d_{5/2}$ configurations have been extended up to $(16)^-$ and $(13)^+$ states, respectively. A new $\Delta I = 1$ band was identified, and interpreted in terms of the triaxial particle rotor model calculations.

DOI: 10.1103/PhysRevC.86.064302 PACS number(s): 21.10.Re, 27.60.+j, 23.20.Lv, 21.60.Ev

I. INTRODUCTION

The studies of antimony ($_{51}$Sb) isotopes have provided a wealth of interesting physics [1–3]. Not only were single-particle levels observed in the energy spectra, but also collective levels were found at high excitation energies. In this mass region, the coexistence between single-particle and collective levels is well understood in terms of the preference for spherical shape at low excitation energy, owing to the proximity of the $Z = 50$ shell gap, and the preference for a deformed shape at higher excitation energies, when protons are promoted from the β-upsloping $g_{9/2}$ orbital into the β-downsloping $g_{7/2}$ orbital. Such particle-hole excitations are known to result in collective rotational bands in the antimony [4–10] and tin [11–14] isotopes. These nuclei thus provide an ideal laboratory for exploring the competition between the single-particle and collective degrees of freedom. So far, the available information on ^{116}Sb is limited compared to many of its neighbors in this mass region. Motivated by these considerations, experiments were performed to investigate high-spin states of ^{116}Sb using the standard in-beam γ-ray spectroscopy techniques. Prior to this work, low-spin states of ^{116}Sb were studied via the radioactive-decay technique [15], and using the ^{116}Sn(p, n) [16] and ^{113}In(α,n) [17–19] reactions. High-spin states of ^{116}Sb were also investigated by the ^{113}Cd(^{7}Li, 4n) reaction [8].

II. EXPERIMENT

Excited states in ^{116}Sb were populated using the ^{114}Cd(^{7}Li, $5n$) fusion-evaporation reaction at a beam energy of 48 MeV using the HI-13 tandem accelerator at the China Institute of Atomic Energy (CIAE) in Beijing. A self-supporting target composed of two stacked 2.5 mg/cm^2 metallic foils was used. γ-γ coincidences were measured with an array consisting of 12 Compton-suppressed high-purity germanium (HPGe)-bismuth germanate (BGO) detectors and two planar-type HPGe detectors. Under this condition, a total of 120 million events were collected and used in the offline analysis. The energy and efficiency calibrations of the detectors were made using ^{60}Co and ^{152}Eu standard sources. The typical energy resolution was about 2.2 keV at full width at half maximum (FWHM) for the 1332.5-keV γ-ray. After gain matching, the coincidence data were sorted into a symmetrized E_γ-E_γ matrix and an asymmetric directional correlation of oriented states (DCO) matrix. The symmetrized matrix was used to establish coincidence and intensity relationships for various γ-rays. The dipole-quadrupole nature of the γ-rays was inferred from the analysis of the DCO matrix, which helped in the multipolarity assignments for newly observed rays. In the present array geometry, the DCO ratios turned out to be larger than 1.0 for stretched quadrupole transitions, and less than 0.8 for pure dipole transitions, when gating on a quadrupole transition. The validity of the methods of the DCO measurements were checked from the known transitions in ^{116}Sn [20], which were also produced in the present experiment. The γ-ray energies, their intensities, DCO values, and spin-parity assignments of the excited levels in ^{116}Sb are given in Table I.

III. RESULTS AND DISCUSSIONS

The level scheme of ^{116}Sb obtained from the present work is shown in Fig. 1. The placement of the γ rays in the level scheme is determined through a combination of γ-ray coincidence relationships, intensity balances, and energy sums. As shown in Fig. 1, the level scheme can be roughly separated into two independent parts, exhibiting the coexistence of single-particle and collective structures.

*sywang@sdu.edu.cn

TABLE I. Energies, relative intensities, initial and final spin states, and DCO ratios for observed γ-rays in ^{116}Sb. The intensities are normalized to the 1184.0-keV transition with $I_\gamma = 100$.

E_γ (keV)	I_γ(%)	$I_i^\pi \longrightarrow I_f^\pi$	DCO ratio
99.8	12.2(1.9)	$8^- \rightarrow 7^-$	
143.2	<2	$13^+ \rightarrow (12)^+$	
192.6	28.8(4.0)	$7^- \rightarrow 7^+$	0.83(0.43)
215.0	82.0(10.2)	$9^- \rightarrow 8^-$	0.95(0.34)
226.3	18.1(2.5)	$15^+ \rightarrow 14^+$	
240.8	34.1(4.6)	$14^+ \rightarrow 13^+$	0.63(0.17)
273.6	16.5(2.1)	$8^+ \rightarrow 7^-$	
298.1	10.5(1.6)	$(13)^+ \rightarrow (12)^+$	0.75(0.18)
317.2	99.1(7.3)	$10^- \rightarrow 9^-$	0.65(0.14)
324.4	30.7(3.1)	$9^+ \rightarrow 8^+$	0.32(0.11)
339.9	50.9(4.1)	$(13)^- \rightarrow (12)^-$	0.76(0.17)
349.7	19.4(3.2)	$7^+ \rightarrow 7^-$	
352.2	91.3(6.9)	$11^- \rightarrow 10^-$	0.92(0.48)
361.1	7.6(1.3)	$(18^+) \rightarrow$	
365.2	31.3(3.2)	$10^+ \rightarrow 9^+$	0.64(0.15)
374.3	9.3(1.2)	$11^+ \rightarrow 10^+$	
382.4	59.8(4.6)	$12^- \rightarrow 11^-$	0.71(0.2)
389.4	46.5(3.9)	$(14)^- \rightarrow (13)^-$	0.67(0.18)
391.2	39.9(3.6)	$9^+ \rightarrow 8^+$	0.59(0.35)
405.1	32.2(2.8)	$10^+ \rightarrow 9^+$	0.89(0.16)
410.8	37.9(3.4)	$13^- \rightarrow 12^-$	0.83(0.27)
411.0	64.4(5.3)	$8^+ \rightarrow 7^+$	1.05(0.20)
423.7	24.1(3.1)	$11^+ \rightarrow 10^+$	1.1(0.32)
423.7	9.1(2.2)	$(13)^+ \rightarrow (12)^+$	
426.1	49.5(3.9)	$7^- \rightarrow 8^-$	0.67(0.15)
430.2	35.0(3.0)	$(15)^- \rightarrow (14)^-$	0.81(0.28)
435.7	21.4(2.5)	$(12)^+ \rightarrow 11^+$	0.83(0.29)
444.0	31.0(2.6)	$14^- \rightarrow 13^-$	0.54(0.2)
463.2	33.6(3.1)	$(16)^- \rightarrow (15)^-$	0.68(0.31)
467.1	41.3(3.5)	$15^+ \rightarrow 13^+$	1.14(0.16)
467.2	32.4(3.2)	$8^+ \rightarrow 7^+$	1.21(0.43)
485.7	21.6(2.0)	$(17)^- \rightarrow (16)^-$	
494.3	18.9(1.7)	$(15)^- \rightarrow 14^-$	0.39(0.23)
507.2	23.2(1.9)	$(16)^+ \rightarrow 15^+$	3.25(0.59)
526.8	14.5(1.6)	$(16)^- \rightarrow (15)^-$	
532.2	8.9(1.1)	$10^- \rightarrow 8^-$	0.92(0.48)
532.6	12.8(1.8)	$(18^+) \rightarrow (17)^+$	0.51(0.13)
542.3	30.2(4.2)	$7^- \rightarrow 7^-$	
558.2	9.8(1.7)	$\rightarrow 11^+$	
597.4	30.0(3.3)	$(16)^+ \rightarrow 14^+$	1.52(0.33)
597.6	8.2(1.6)	$(13)^+ \rightarrow (12)^+$	
625.2	4.2(1.4)	$10^- \rightarrow 9^-$	
642.0	17.4(2.2)	$8^- \rightarrow 7^-$	
646.6	25.5(2.9)	$11^+ \rightarrow 9^-$	1.47(0.35)
667.7	10.1(1.2)	$\rightarrow 15^+$	
669.4	16.6(2.9)	$(12)^- \rightarrow 11^-$	
669.6	19.6(2.3)	$11^- \rightarrow 9^-$	0.99(0.39)
679.2	<2	$\rightarrow (12)^+$	
689.9	8.1(1.5)	$10^+ \rightarrow 8^+$	2.05(0.92)
728.4	14.2(1.7)	$(18^+) \rightarrow (16)^+$	1.73(0.52)
733.8	5.5(1.2)		
734.7	11.1(1.3)	$\rightarrow (13)^+$	
734.8	18.4(2.3)	$12^- \rightarrow 10^-$	1.05(0.44)
739.3	6.8(1.4)	$11^+ \rightarrow 9^+$	0.25(0.17)
752.5	35.0(4.0)	$9^- \rightarrow 8^-$	2.81(0.77)
775.8	23.1(2.8)	$7^+ \rightarrow 8^-$	1.56(0.54)
793.2	17.8(2.3)	$13^- \rightarrow 11^-$	0.92(0.49)
796.1	11.8(1.7)	$10^+ \rightarrow 8^+$	11.8(1.7)
802.2	17.8(2.5)	$9^+ \rightarrow 7^+$	17.8(2.5)
812.3	21.7(2.6)	$(17)^+ \rightarrow 15^+$	1.33(0.34)
828.4	11.8(1.7)	$11^+ \rightarrow 9^+$	
837.1	5.3(0.8)	$(18^+) \rightarrow (16)^+$	
854.8	15.5(1.6)	$14^- \rightarrow 12^-$	0.92(0.25)
859.1	11.9(1.2)	$(12)^+ \rightarrow 10^+$	1.59(0.77)
859.6	16.0(1.6)	$(13)^+ \rightarrow 11^+$	1.59(0.77)
893.9	11.1(1.3)	$(17)^+ \rightarrow 15^+$	1.44(0.44)
933.2	5.9(0.9)	$\rightarrow 14^+$	
938.4	9.4(1.0)	$(15)^- \rightarrow 13^-$	1.42(0.7)
968.4	62.8(5.6)	$7^- \rightarrow 8^-$	1.97(0.50)
983.2	5.8(0.7)	$\rightarrow 15^+$	
1009.2	5.0(0.6)	$\rightarrow (17)^+$	0.81(0.37)
1021.2	10.1(1.0)	$(16^-) \rightarrow 14^-$	7.59(4.86)
1021.5	<3	$\rightarrow 9^-$	
1021.6	62.5(5.7)	$(12)^- \rightarrow 10^-$	
1041.3	7.3(0.8)	$(12)^+ \rightarrow 11^+$	0.27(0.06)
1068.0	10.1(1.1)	$8^- \rightarrow 8^-$	
1170.4	11.0(1.8)	$(12)^+ \rightarrow 11^+$	0.31(0.11)
1184.0	100	$13^+ \rightarrow 11^+$	1.09(0.18)
1248.8	4.1(0.5)	$\rightarrow 9^-$	
1283.6	16.8(1.7)	$9^- \rightarrow 8^-$	
1350.9	<3	$\rightarrow 9^-$	
1377.6	8.1(0.9)	$10^- \rightarrow 8^-$	1.13(0.31)
1399.1	88.6(7.2)	$11^+ \rightarrow 8^-$	0.85(0.15)
1469.2	12(2.1)	$(12)^+ \rightarrow 11^+$	0.53(0.19)

A. Noncollective states

The left-hand side of Fig. 1 reveals a number of irregular levels arising from the particle excitations. The present work extended these levels to an excitation energy of ~5 MeV with spin 18$\hbar$ by adding about 22 new transitions. Most of the new transitions can be clearly seen in Figs. 2(a) and 2(b).

A common feature for most of the odd-odd antimony isotopes is an isomeric state with $I^\pi = 8^-$ (see Ref. [6] and references therein). In the present work, all reported γ rays feed eventually towards this isomeric state. Magnetic and quadrupole moment measurements have shown that this isomer is formed from the $\pi d_{5/2} \otimes \nu h_{11/2}$ configuration [21]. Multiquasiparticle excitations, such as the coupling of the quasiproton in the $d_{5/2}$, $g_{7/2}$, or $h_{11/2}$ orbit to the quasineutron $h_{11/2}$, play an important role in building the single-particle levels in ^{116}Sb. Thus, it is expected that the next high-spin two-quasiparticle (2qp) states should be associated with the $\pi g_{7/2} \otimes \nu h_{11/2}$ and $\pi h_{11/2} \otimes \nu h_{11/2}$ configurations. Such 2qp multiplets should be yrast and easy to observe using the heavy-ion fusion-evaporation reactions. With these features in mind, the low-lying 9_1^- state at 1135.5 keV and 11_1^+ state at 1782.1 keV in ^{116}Sb may be assigned to be the $\pi g_{7/2} \otimes \nu h_{11/2}$ and $\pi h_{11/2} \otimes \nu h_{11/2}$ configurations, respectively.

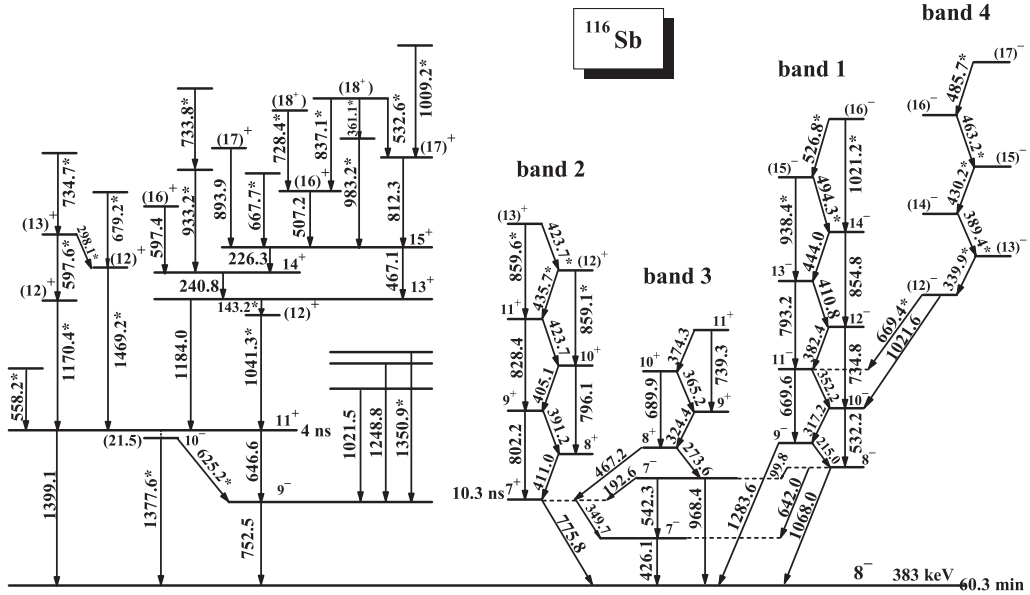

FIG. 1. Level scheme of ^{116}Sb proposed in the present work. New transitions observed in the present work are denoted with asterisks.

Another feature common to the odd-odd Sb isotopes is a low-lying 10^- state. The 10^- state had been explained as the 2^+ excitation in the even Sn isotopes coupled to the lowest-lying 8^- isomer. These low-lying 10^- states have systematically been observed in ^{110,112,114}Sb [5–7] and ^{118,120}Sb [9,22]. A similar state is expected in ^{116}Sb. However, no low-lying 10^- single-particle level was reported in ^{116}Sb. In the present work, a new 1377.6-keV transition belonging to ^{116}Sb is identified. This 1377.6-keV transition is in coincidence with the transitions above the 11^+_1 state at 1782.1 keV, but not with the 1399.1-keV transition [see Figs. 2(a) and 2(b)]. Hence, the 1377.6-keV transition was placed in parallel with the 1399.1-keV transition in the present level scheme. The 1377.6-keV transition is most probably directly feeding the 8^- isomer. This may be corroborated by the observation of the 625.2-keV transition linking this level at 1867.6 keV into the yrast 9^- level at 1135.5 keV. The measured DCO ratio for the 1377.6-keV transition is consistent with the stretched electric quadrupole character. On this basis we introduced a new level at 1867.6 keV, which is most likely the missing 10^- yrast state. The occurrence of the 1377.6-keV transition also implies an unobserved $11^+ \rightarrow 10^-$ $E1$ transition of 21.5 keV.

Figure 3 presents the systematics of the excitation energies for the 8^-_1, 10^-_1, and 11^+_1 levels in ^{110,112,114,116,118,120}Sb [5–9,22]. For comparison, the 0^+_1 and 2^+_1 levels in ^{108,110,112,114,116,118}Sn [11–14] are also included. As shown in Fig. 3, the excitation energies of $I^\pi = 10^-_1$ in odd-odd Sb isotopes show the same trend as those of $I^\pi = 2^+_1$ in

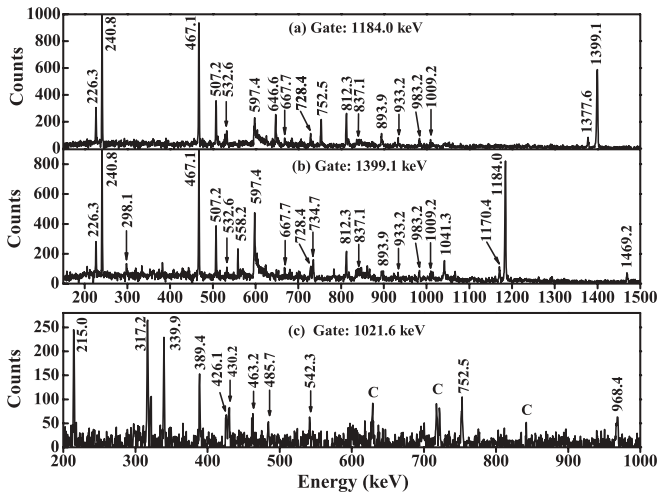

FIG. 2. Coincidence spectra obtained by gating on (a) the 1184.0-keV transition, (b) the 1399.1-keV transition, and (c) the 1021.6-keV transition. The peaks labeled C indicate contaminations.

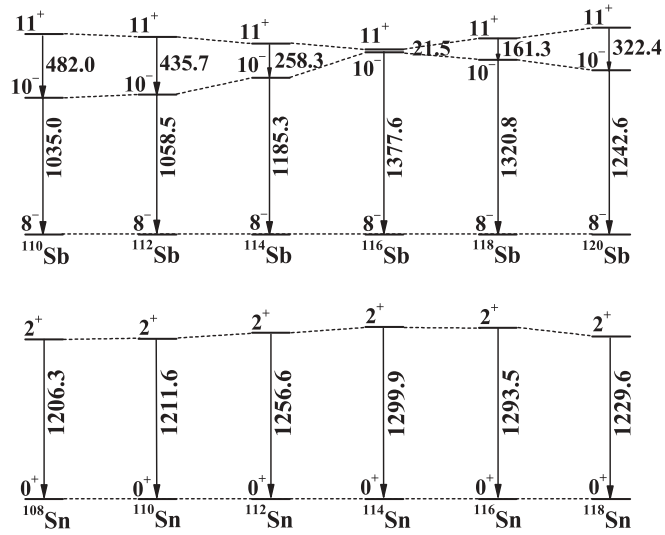

FIG. 3. Energy systematics of the 8^-_1, 10^-_1, and 11^+_1 states in ^{110,112,114,116,118,120}Sb compared to the 0^+_1 and 2^+_1 states in ^{108,110,112,114,116,118}Sn. Data are taken from Refs. [5–14,22] and the present work.

even-even Sn isotopes. The 10_1^- state in ^{116}Sb fits well into the systematics of the odd-odd Sb isotopes. Furthermore, the excitation energies of the 10_1^- levels in Sb isotopes exhibit parabolic shapes with a maximum energy at the center of the neutron shell ($N = 66$), whereas 11_1^+ levels exhibit a minimum energy at $N = 66$. This leads to a small energy gap between 10_1^- and 11_1^+ levels in ^{116}Sb. These facts provide further support for the present placements of the 1377.6- and 21.5-keV transitions.

Above the 11_1^+ state at 1782.1 keV, the present work confirms the previously reported placements of transitions and spin-parity assignments of levels, and adds about 18 new transitions into the level scheme. For these new transitions, the DCO results suggest stretched quadrupole character for the 597.4-, 728.4-, 812.3-, and 893.9-keV transitions and stretched dipole character for the 298.1-, 532.6-, 1041.3-, 1170.4-, and 1469.2-keV transitions, giving the current spin-parity assignments shown in Fig. 1. In the odd-odd nucleus ^{116}Sb, the maximum angular momentum formed in a two-quasiparticle configuration is 11^+, and therefore the higher-spin states above 11^+ should be associated with the coupling of two-quasiparticle multiplets to the core excitations.

B. Collective structures

On the right-hand side of Fig. 1, four strongly coupled bands are constructed and labeled 1, 2, 3, and 4. For bands 1, 2, and 3, which were observed prior to this work, the proposed spin and parity assignments to levels are partially determined by the DCO ratios and the previously known low spin levels reported by Refs. [8,19].

Band 1 is the most strongly populated rotational band in ^{116}Sb, and was already assigned as the $\pi {g_{9/2}}^{-1} \otimes \nu h_{11/2}$ configuration [17]. In the present work, band 1 was extended from $I^\pi = (14)^-$ to $(16)^-$. Band 2 was also extended up to $I^\pi = (13)^+$. In Ref. [19], band 2 and band 3 were proposed to be built predominantly on the $\pi {g_{9/2}}^{-1} \otimes \nu d_{5/2}$ and $\pi {g_{9/2}}^{-1} \otimes \nu g_{7/2}$ configurations, respectively. Therefore, bands 2 and 3 could be interpreted as a pair of pseudospin partners. The similar doublet bands were observed in neighboring ^{118}Sb [9]. In addition, a new $\Delta I = 1$ band (labeled band 4) was identified in parallel to the yrast band. A sample spectrum for this band is shown in Fig. 2(c). The placement of band 4 in the level scheme was determined on the basis of two γ rays with energies of 669.4 and 1021.6 keV, which connect this band with band 1. The 1021.6-keV transition was reported in the previous work [8], but no multipolarity assignment was given at that time. Unfortunately, the DCO ratios for 669.4- and 1021.6-keV transitions cannot be obtained accurately in the present work, owing to the unresolved doublets. According to the general yrast argument, an increasing spin with increasing excitation energy was assumed. Thus, we adopted $I = 12\hbar$ for the lowest observed state of band 4. The positive-parity assignment can be ruled out because it would require an $M2$ multipolarity for the 1021.6-keV transition, which would not compete with the presumed 669.4-keV $E1$ transition. Thus, the $I^\pi = 12^-$ is tentatively assigned for the lowest observed state of band 4.

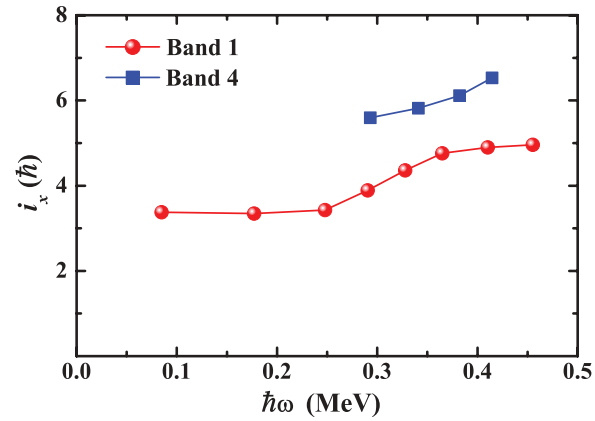

FIG. 4. (Color online) Experimental alignment plots for the bands in ^{116}Sb. The Harris parameters $J_0 = 17\hbar^2$ MeV^{-1} and $J_1 = 12\hbar^4$ MeV^{-3} were used.

To assign the configuration of band 4, the aligned angular momenta for bands 1 and 4 are extracted and plotted in Fig. 4 using the spins marked on the level scheme in Fig. 1. The large alignment and the high excitation energy suggest that band 4 would be the four-quasiparticle band structure. Band 4 has strong $\Delta I = 1$ transitions with absent $\Delta I = 2$ crossover transitions and small signature splitting. Thus, the $\pi g_{9/2}$ hole should be part of the band configuration. The obvious possibility to consider is the $\pi g_{9/2}$ hole coupled to a three-quasineutron configuration, since the presence of the $Z = 50$ shell gap makes a three-quasiproton configuration unlikely. As shown in Fig. 4, band 4 has a large initial alignment of $\sim 6\hbar$. The large alignment strongly suggests that the $h_{11/2}$ neutron must be involved in the configuration of band 4. Taking the above information into account, we propose band 4 to be based on the $\pi(g_{9/2})^{-1} \otimes \nu h_{11/2}(g_{7/2}/d_{5/2})^2$ configuration. The band built on the $\pi(g_{9/2})^{-1} \otimes \nu h_{11/2}(g_{7/2}/d_{5/2})^2$ configuration would have approximately $5\hbar \sim 7\hbar$ of aligned angular momentum, consistent with the present experimental observations. This configuration assignment can be also supported by the following particle-rotor model (PRM) calculations.

A triaxial n-particle–n-hole PRM was developed and used for the description of chiral doublet bands of ^{135}Nd [23] and ^{103,105}Rh [24]. In the present work, we performed the n-particle–n-hole PRM calculations for band 4 on the basis of the proposed $\pi(g_{9/2})^{-1} \otimes \nu h_{11/2}(g_{7/2}/d_{5/2})^2$ configuration. The configuration-fixed constrained triaxial relativistic mean-field (RMF) approaches were applied to determine the deformations for band 4 with parameter set PC-PK1 [25]. A detailed description of this approach can be found in Ref. [26] and references therein. Self-consistent deformation parameters $\beta_2 = 0.15$ and $\gamma = 33.9^\circ$ are obtained from the present RMF approaches corresponding to the $\pi(g_{9/2})^{-1} \otimes \nu h_{11/2}(g_{7/2}/d_{5/2})^2$ configuration in ^{116}Sb. Accordingly, the coupling parameter C in the Hamiltonian of the single-j shell is defined as $C(g_{9/2}) = -0.265$, $C(h_{11/2}) = 0.217$, and $C(g_{7/2}/d_{5/2}) = 0.477$ MeV [27]. For the calculation of electromagnetic transitions, the intrinsic quadrupole moment Q_0 is taken to be $(3/\sqrt{5\pi})R_0^2 Z\beta = 1.725$ eb. Gyromagnetic ratios

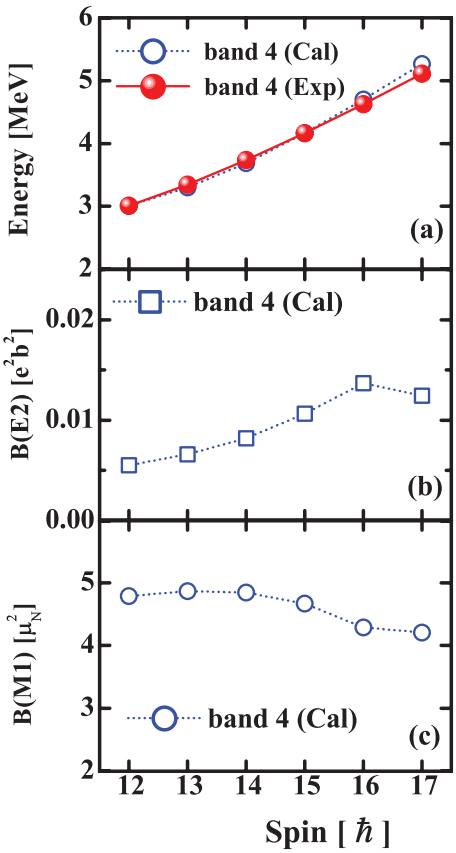

FIG. 5. (Color online) Plot of the excitation energies $E(I)$, $B(M1)$, and $B(E2)$ values for band 4 as a function of spin. The solid (open) symbols are for the experimental (calculated) values. The calculated values are shifted to coincide with the experimental energy at the bandhead.

$g_R = Z/A \approx 0.44$, $g(\pi g_{9/2}) = 1.261$, $g(\nu h_{11/2}) = -0.209$, and $g(\nu g_{7/2}/d_{5/2}) = -0.459$ were adopted.

In Fig. 5(a), the calculated energy spectra $E(I)$ for band 4 is compared with the corresponding experimental results. As shown in Fig. 5(a), the calculations well reproduce the energy levels of band 4. This gives us more confidence on the configuration assignment for band 4. To compare with future lifetime data, the reduced $B(M1)$ and $B(E2)$ transition probabilities are calculated and presented in Figs. 5(b) and 5(c), respectively. The calculated $B(E2)$ values are small ($\sim$0.01 e^{2}b^2), whereas the $B(M1)$ values are relatively large ($\sim 4.5\mu_N^2$). These are consistent with the present experimental observations.

Another interesting feature in this mass region is the magnetic rotational band. Recently, lots of experimental and theoretical effort was made to search for Refs. [28–30] and to interpret [31–34] this phenomenon. Magnetic rotational bands were observed in even-even ^{106,108}Sn [35,36], odd-A ^{105}Sn [37], and odd-odd ^{108}Sb [4] in this mass region. Band 4 contains strong $\Delta I = 1$ transitions, and no crossover transitions between $\Delta I = 2$ states were observed within our statistical limits. Thus, band 4 would expect to be a magnetic rotational band. The behavior of $B(M1)$ values can be used to distinguish between the shears mechanism and the rotation of the core. If the angular momentum is purely built from the shears mechanism, then the $B(M1)$ values are expected to decrease as the angular momentum increases. However, if the angular momentum is generated by the rotation of the core alone, then the $B(M1)$ values should essentially remain constant with spin [36,38]. As shown in Fig. 5(c), the calculated $B(M1)$ values show a slight decrease with increasing spin. It implies that the shears mechanism is not a very dominant contribution to the generation of angular momentum for band 4. Therefore, seemingly band 4 should exist in the strong competition between the shear mechanism and collective rotation. To give more direct experimental evidence, precise lifetime measurements for band 4 in ^{116}Sb are highly desirable.

IV. SUMMARY

In summary, excited states of ^{116}Sb were investigated using in-beam γ-ray spectroscopy techniques with the ^{114}Cd(^{7}Li, $5n$) reaction. The level scheme of ^{116}Sb was extended by adding about 25 new states and 35 new transitions. The previously known two rotational bands based on the $\pi {g_{9/2}}^{-1} \otimes \nu h_{11/2}$ and $\pi {g_{9/2}}^{-1} \otimes \nu d_{5/2}$ configurations were extended up to $(16)^-$ and $(13)^+$ states, respectively. A new $\Delta I = 1$ band was identified and assigned as the $\pi(g_{9/2})^{-1} \otimes \nu h_{11/2}(g_{7/2}/d_{5/2})^2$ configuration.

ACKNOWLEDGMENTS

This study is supported by the National Natural Science Foundation (Grants No. 11175108, No. 11005069, and No. 10875074), the Shandong Natural Science Foundation (Grant No. ZR2010AQ005), and the Independent Innovation Foundation of Shandong University (Grant No. 2011ZRYQ004) of China. We express sincere thanks to S. Q. Zhang, P. W. Zhao, and L. F. Yu for providing the deformation calculation and helpful discussions.

[1] V. P. Janzen *et al.*, Phys. Rev. Lett. **70**, 1065 (1993).
[2] V. P. Janzen *et al.*, Phys. Rev. Lett. **72**, 1160 (1994).
[3] R. Wadsworth *et al.*, Phys. Rev. Lett. **80**, 1174 (1998).
[4] D. G. Jenkins *et al.*, Phys. Rev. C **58**, 2703 (1998).
[5] G. J. Lane *et al.*, Phys. Rev. C **55**, R2127 (1997).
[6] G. J. Lane *et al.*, Phys. Rev. C **58**, 127 (1998).
[7] E. S. Paul *et al.*, Phys. Rev. C **50**, 2297 (1994).
[8] R. Duffait, J. van Maldeghem, A. Charvet, J. Sau, K. Heyde, A. Emsallem, M. Meyer, R. Beraud, J. Treherne, and J. Genevey, Z. Phys. A **307**, 259 (1982).
[9] S. Y. Wang *et al.*, Phys. Rev. C **82**, 057303 (2010).
[10] S. Vajda, W. F. Piel, Jr., M. A. Quader, W. A. Watson, F. C. Yang, and D. B. Fossan, Phys. Rev. C **27**, 2995 (1983).
[11] J. Bron *et al.*, Nucl. Phys. A **318**, 335 (1979).

[12] D. A. Viggars, H. W. Taylor, B. Singh, and J. C. Waddington, Phys. Rev. C **36**, 1006 (1987).
[13] S. Juutinen *et al.*, Nucl. Phys. A **617**, 74 (1997).
[14] S. Y. Wang *et al.*, Phys. Rev. C **81**, 017301 (2010).
[15] C. B. Morgan, W. H. Bentley, R. A. Warner, W. H. Kelly, and Wm. C. McHarris, Phys. Rev. C **23**, 1228 (1981).
[16] Z. Gácsi, T. Fenyes, and Zs. Dombrádi, Phys. Rev. C **44**, 626 (1991).
[17] P. Van Nes *et al.*, Nucl. Phys. A **379**, 35 (1982).
[18] Z. Gácsi, Zs. Dombrádi, T. Fényes, S. Brant, and V. Paar, Phys. Rev. C **44**, 642 (1991).
[19] M. Fayez-Hassan *et al.*, Nucl. Phys. A **624**, 401 (1997).
[20] A. Savelius *et al.*, Nucl. Phys. A **637**, 491 (1998).
[21] P. T. Callaghan, M. Shott, and N. J. Stone, Nucl. Phys. A **221**, 1 (1974).
[22] K. Kitao, Y. Tendow, and A. Hashizume, Nucl. Data Sheets **96**, 241 (2002).
[23] B. Qi, S. Q. Zhang, J. Meng, S. Y. Wang, and S. Frauendorf, Phys. Lett. B **675**, 175 (2009).
[24] B. Qi, S. Q. Zhang, S. Y. Wang, J. Meng, and T. Koike, Phys. Rev. C **83**, 034303 (2011).
[25] P. W. Zhao, Z. P. Li, J. M. Yao, and J. Meng, Phys. Rev. C **82**, 054319 (2010).
[26] J. Meng, J. Peng, S. Q. Zhang, and S. G. Zhou, Phys. Rev. C **73**, 037303 (2006).
[27] S. Y. Wang, B. Qi, and S. Q. Zhang, Chin. Phys. Lett. **26**, 052102 (2009).
[28] R. M. Clark *et al.*, Phys. Rev. Lett. **78**, 1868 (1997).
[29] H. Schnare *et al.*, Phys. Rev. Lett. **82**, 4408 (1999).
[30] R. Schwengner *et al.*, Phys. Rev. C **66**, 024310 (2002).
[31] S. Frauendorf and J. Meng, Z. Phys. A **356**, 263 (1996).
[32] J. Peng, J. Meng, P. Ring, and S. Q. Zhang, Phys. Rev. C **78**, 024313 (2008).
[33] P. W. Zhao, S. Q. Zhang, J. Peng, H. Z. Liang, P. Ring, and J. Meng, Phys. Lett. B **699**, 181 (2011).
[34] L. F. Yu, P. W. Zhao, S. Q. Zhang, P. Ring, and J. Meng, Phys. Rev. C **85**, 024318 (2012).
[35] D. G. Jenkins *et al.*, Phys. Lett. B **428**, 23 (1998).
[36] D. G. Jenkins *et al.*, Phys. Rev. Lett. **83**, 500 (1999).
[37] A. Gadea *et al.*, Phys. Rev. C **55**, R1 (1997).
[38] R. M. Clark *et al.*, Phys. Rev. Lett. **82**, 3220 (1999).